arXiv:cond-mat/0604149v1 [cond-mat.supr-con] 5 Apr 2006

BCS-BEC Crossover in Atomic Fermi Gases with a Narrow Resonance

L. M. Jensen[1,2,3], H. M. Nilsen[4], and Gentaro Watanabe[1,5]
[1] *NORDITA, Blegdamsvej 17, DK-2100, Copenhagen Ø, Denmark*
[2] *Department of Physics, Nanoscience Center, P.O. Box 35, FIN-40014 University of Jyväskylä, Finland*
[3] *Department of Theoretical Physics, Umeå University, Umeå, 901 87, Sweden*
[4] *Center for Mathematics for Applications, P.O. Box 1053, Blindern, NO-0316, Oslo Norway*
[5] *The Institute of Chemical and Physical Research (RIKEN), 2-1 Hirosawa, Wako, Saitama 351-0198, Japan*

We determine the effects on the BCS-BEC crossover of the energy dependence of the effective two-body interaction, which at low energies is determined by the effective range. To describe interactions with an effective range of either sign, we consider a single-channel model with a two-body interaction having an attractive square well and a repulsive square barrier. We investigate the two-body scattering properties of the model, and then solve the Eagles-Leggett equations for the zero temperature crossover, determining the momentum dependent gap and the chemical potential self-consistently. From this we investigate the dependence of the crossover on the effective range of the interaction.

PACS numbers: 03.75.Hh,03.75.Ss,03.65.Nk,05.30.Fk

I. INTRODUCTION

Recently there has been remarkable progress in realizing, in ultracold atomic Fermi gases, the crossover from weak-coupling (BCS) superfluidity to Bose-Einstein condensation (BEC) of bound diatomic molecules. The key to this development is that, due to Feshbach molecular resonances, the strength and sign of the effective interatomic interaction can be tuned by varying the external magnetic field. For positive scattering lengths the resonantly enhanced interaction has been used to create a long-lived gas of diatomic molecules and Bose-Einstein condensates of molecules. For a negative scattering length, experimental evidence has been obtained for an atom-pair correlated state analogous to the BCS superconducting state at weak coupling [1, 2]. Additional studies of collective modes [3, 4] and the spectroscopic pairing gap [5] in the crossover region also display behavior consistent with pairing, the most convincing experiment to date being the observation of a vortex lattice in the entire BCS-BEC crossover region [6].

The simplest model describing the crossover is due to Eagles and Leggett [7, 8, 9], in which the effective fermion-fermion interaction is parametrized by the scattering length, a. This approximation for the interaction is valid as long as the effective fermion-fermion interaction does not vary significantly on the scale of the Fermi energy, E_{F}, the energy relevant for the many-body problem [10, 11]. In practice, large scattering lengths are realized by using Feshbach resonances, and resonances for which this condition holds are referred to as “broad”. For such resonances, the atom-molecule coupling and the width parameter for the resonance are large. In the opposite case, the resonance is referred to as “narrow”. Most experiments on the crossover to date have been performed with broad resonances. For the resonance in ^{6}Li, the experimental data on the evolution of condensate profile [12] agrees well with the universal single-channel model [13, 14]. In [3, 4] measurements of the collective axial and radial modes of a trapped ^{6}Li gas were reported to be quantitatively in agreement with results obtained from the zero temperature BCS-BEC crossover [15, 16].

In the future, one may anticipate that experiments will be made on the crossover for narrow resonances. It is therefore of interest to investigate the influence of energy dependence of the interaction on the crossover. The leading contributions to the effective interaction beyond the scattering length are expressed in terms of the effective range, r_e, which is defined in terms of the s-wave scattering phase shift δ by the equation

$$k\cot\delta = -\frac{1}{a} + \frac{1}{2}r_e k^2 + O(k^4), \tag{1}$$

where k is the wave number for the relative motion. The influence of the effective range is also interesting from the point of view of the BCS-BEC crossover produced by varying the density of the gas [17]. In this case, the effective interaction between atoms at the Fermi surface depends on the Fermi momentum, and hence depends on density. Several approaches to study effective range dependence are based on microscopic interaction potentials, e.g., coupled square wells [18], the modified Pöschl-Teller potential [19], and the Gaussian potential [17, 20]. For monotonic attractive potentials the effective range is positive and can be shown to be related to an average range of the microscopic potential. The effective range expansion applied to the multichannel scattering problem yields effective ranges of either sign. In Refs. [21, 22] the properties of a square well plus square barrier model potential were matched with the scattering properties of a renormalized two-channel resonance model [23] and the zero temperature atom-molecule BCS-BEC crossover was re-expressed in terms of an effective single-channel potential model with a large and negative effective range [10, 21].

The purpose of this paper is to investigate the dependence of the crossover on the energy dependence of the effective two-body interaction. We shall start from a microscopic model, a square-well, square-barrier potential, which has previously been employed in Ref. [21]. This can be used to construct effective interactions with different scattering lengths and an effective range that can be either positive or negative. We then solve the Eagles-Leggett equations, determining the gap and the chemical potential self-consistently. Non-trivial corrections due to the negative effective range have not been fully investigated so far and such calculations provide a useful guide to explore the BCS-BEC crossover for narrow resonances in the future.

The paper is organized as follows: Section II contains a general introduction to the low energy effective range expansion of the effective interatomic interaction in a dilute Fermi gas [24, 25]. In Section III the two-body properties of the square-well, square-barrier potential are derived. Subsequently, in Section IV we numerically solve the zero temperature BCS-BEC crossover problem using the Eagles-Leggett variational state [7, 8] and re-express the crossover properties in terms of the low energy two-body properties.

II. EFFECTIVE RANGE EXPANSION

Historically, the effective range expansion originated in attempts to understand nuclear forces from low energy nucleon scattering experiments [24, 25]. Classical problems such as nucleon-nucleon scattering, the deuteron spectrum, and α decay were studied by such methods. Recently, the effective range was introduced to the field of ultracold atom gases where its size and sign are related to the width of the Feshbach resonances.

The dominant scattering process in an ultracold two-component Fermi gas is the binary elastic s-wave scattering between the atoms. When the typical wavelength λ corresponding to the collision energy $E \sim \hbar^2/m\lambda^2$ (m is the mass of the fermion atom) is much larger than the range of the inter-atomic potential $U(\mathbf{r})$, this process, in the center-of-mass frame, can be described by the Schrödinger equation with a radial wave function $r\psi$ of the s-state:

$$-\frac{\hbar^2}{m}\nabla^2\psi(\mathbf{r}) + U(\mathbf{r})\psi(\mathbf{r}) = E\psi(\mathbf{r}). \tag{2}$$

Let us consider an interatomic potential with a finite range r_1, i.e., $U(r) = 0$ at $r > r_1$. Using the solutions ψ_1 and ψ_2 of Eq. (2) with the energies $E_i = \hbar^2 k_i^2/m$ $(i = 1, 2)$, we get

$$\left[\psi_2\frac{d\psi_1}{dr} - \psi_1\frac{d\psi_2}{dr}\right]_0^{r_1} = (k_2^2 - k_1^2)\int_0^{r_1}\psi_1\psi_2 dr. \tag{3}$$

Following Bethe [25], we introduce a reference wave function $\psi_{\mathrm{ref},i}$ which coincides with ψ_i outside the potential:

$$\psi_{\mathrm{ref},i} = \sin(k_i r + \delta_i), \tag{4}$$

where δ_i is the phase shift for energy E_i. For the reference wave functions, a similar relation to Eq. (3) holds

$$\begin{aligned}&\left[\psi_{\mathrm{ref},2}\frac{d\psi_{\mathrm{ref},1}}{dr} - \psi_{\mathrm{ref},1}\frac{d\psi_{\mathrm{ref},2}}{dr}\right]_0^{r_1} \\ &= (k_2^2 - k_1^2)\int_0^{r_1}\psi_{\mathrm{ref},1}\psi_{\mathrm{ref},2}dr.\end{aligned} \tag{5}$$

Subtracting Eq. (3) from Eq. (5) leads to

$$\begin{aligned}&\left(\psi_{\mathrm{ref},1}\frac{d\psi_{\mathrm{ref},2}}{dr} - \psi_{\mathrm{ref},2}\frac{d\psi_{\mathrm{ref},1}}{dr}\right)_{r=0} \\ &= (k_2^2 - k_1^2)\int_0^{r_1} dr\ (\psi_{\mathrm{ref},1}\psi_{\mathrm{ref},2} - \psi_1\psi_2)\ .\end{aligned} \tag{6}$$

Then we take $k_1 = 0$ and use the relation

$$\lim_{k_1\to 0} k_1 \cot\delta_1 = -\frac{1}{a} \tag{7}$$

for the s-wave scattering length a to write

$$k\cot\delta = -\frac{1}{a} + \frac{1}{2}k^2\rho(k), \tag{8}$$

with

$$\rho(k) \equiv 2\int_0^{r_1} dr\left(\frac{\psi_{\mathrm{ref},0}}{\sin\delta_0}\frac{\psi_{\mathrm{ref}}}{\sin\delta} - \frac{\psi_0}{\sin\delta_0}\frac{\psi}{\sin\delta}\right), \tag{9}$$

here we use the subscripts zero for the state with $k = 0$ and we omit the subscripts 2.

Comparing Eqs. (1) and (8), we get

$$r_e = \rho(k=0) = 2\int_0^{r_1} dr\left(1 - \frac{\psi_0^2}{\sin^2\delta_0}\right). \tag{10}$$

On resonance ($\sin\delta_0 = 1$), the above equation can be written as

$$r_e = r_{e0} = 2\int_0^{r_1} dr(1 - \psi_0^2), \tag{11}$$

here we introduce r_{e0} denoting the effective range at resonance.

In the case of the square-well potential with depth $U_0 = \hbar^2 k_0^2/m$, $\psi_0(r) = \sin(k_0 r)$ for $r < r_1$ with $k_0 r_1 = (n + \frac{1}{2})\pi$ for $(n = 0, 1, 2, \cdots)$ at resonance. Thus we get $r_{e0} = r_1$ for the square-well potential. However, the right hand side of Eq. (11) is different from r_1 for general potentials with a finite range. As will be seen later, both positive and negative r_{e0} can be obtained using a square-well, square-barrier potential.

On resonance ($\delta_0 = \pi/2$), the amplitude of the wave function for $r < r_1$ becomes significant and it can be comparable to or greater than that outside the potential. From Eq. (11) we see that, while for positive r_{e0} the amplitude inside the potential is suppressed relative to that outside, for negative r_{e0} the former is enhanced compared to the latter. Although the effect of r_e is small away from resonance due to the first term on the right hand side of Eq. (1) being much larger than the second one, the sign of r_e has important implications for the behavior of the wave function at resonance.

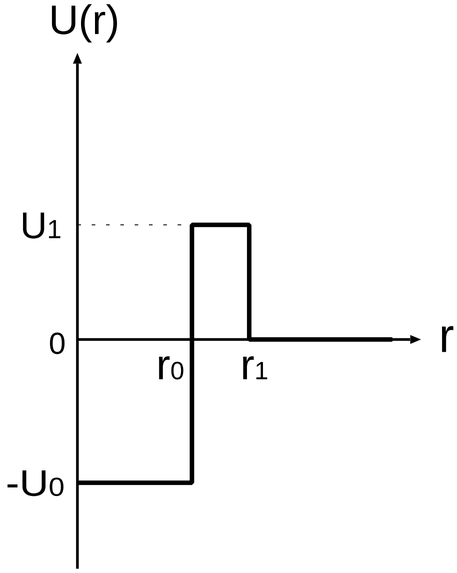

Figure 1: Schematic picture of the square-well, square-barrier potential. We take $U_0, U_1 > 0$ in this paper.

III. SQUARE-WELL, SQUARE-BARRIER MODEL POTENTIAL

We shall model the microscopic interaction by a single-channel potential with a square well and a square barrier. The advantage of this potential, is that it contains the physics necessary to describe resonances: by increasing the thickness of the barrier, or its height, tunneling through the barrier is decreased, and therefore the potential can model the effects of changing the strength of coupling between continuum states and resonant states in the attractive well.

A. Scattering length and effective range

Let us consider two atoms interacting through a step-wise potential with an attractive core of radius $r_0 > 0$ and strength $-U_0 < 0$ and which in addition has a repulsive barrier of width $w = r_1 - r_0$ for $r_1 > r_0$ and a strength $U_1 > 0$ (see Fig. 1):

$$U(r) = \begin{cases} -U_0 & \text{for} \quad 0 \leq r < r_0 \ , \\ U_1 & \text{for} \quad r_0 \leq r < r_1 \ , \\ 0 & \text{for} \quad r_1 \leq r < \infty \ . \end{cases} \tag{12}$$

This problem is solved by the standard method of matching the wave function solutions and their radial derivatives for the above three regions at their respective boundaries, r_0, and r_1 [26].

The general solutions for the three regions are

$$\psi(r) = \begin{cases} A\sin(Kr) & \text{for} \quad 0 \leq r < r_0, \\ B\left(\sinh(\kappa r) + C\cosh(\kappa r)\right) & \text{for} \quad r_0 \leq r < r_1, \\ \sin(kr + \delta) & \text{for} \quad r_1 \leq r < \infty. \end{cases} \tag{13}$$

The well depth parameter is conventionally defined as $k_0^2 = mU_0/\hbar^2$, the barrier height parameter as $k_1^2 = mU_1/\hbar^2$, and the relative kinetic energy of the two colliding particles is $k^2 = mE/\hbar^2$. Furthermore, we introduce the auxiliary parameters $K^2 = m(U_0 + E)/\hbar^2 = k_0^2 + k^2$, and $\kappa^2 = (U_1 - E)/\hbar^2 = k_1^2 - k^2$. The energy dependent s-wave scattering phase shift is denoted by $\delta(k)$. Equating the logarithmic derivatives at the boundaries, the following solutions are found for C and δ. First, C is found from the boundary condition at r_0 to be

$$C = \frac{\kappa\tan(Kr_0) - K\tanh(\kappa r_0)}{K - \kappa\tan(Kr_0)\tanh(\kappa r_0)} \ , \tag{14}$$

and the scattering phase shift is found from the boundary condition at r_1

$$\begin{aligned} \delta(k) =& - kr_1 + \arctan\left(\frac{k}{\kappa}\frac{\tanh(\kappa r_1) + C}{1 + C\tanh(\kappa r_1)}\right) \\ =& - kr_1 + \arctan(\mathcal{R}), \end{aligned} \tag{15}$$

where

$$\mathcal{R}(k) = \frac{k}{\kappa}\frac{\kappa\tan(Kr_0) + K\tanh[\kappa(r_1 - r_0)]}{K + \kappa\tan(Kr_0)\tanh[\kappa(r_1 - r_0)]}. \tag{16}$$

The scattering length is given by

$$\begin{aligned} a =& - \lim_{k\to 0}\frac{\tan\delta(k)}{k} \\ =& r_1 - \frac{1}{k_1\zeta}\left\{k_1\tan(k_0 r_0) + k_0\tanh[k_1(r_1 - r_0)]\right\}, \end{aligned} \tag{17}$$

where

$$\zeta \equiv k_0 + k_1\tan(k_0 r_0)\tanh[k_1(r_1 - r_0)]. \tag{18}$$

In the present work we are also interested in the effective range, which can be derived from the low energy expansion (1) of the phase shift. Expanding $k\cot\delta$ for Eq. (15) to the first order in energy, the first term yields the inverse scattering length as calculated above, and from the second term the following expression for the effective range is obtained:

$$r_e = r_1 + r_{\rm r} + r_{\rm v}, \tag{19}$$

with

$$r_{\rm r} = - \frac{k_0^2 + k_1^2}{k_0 k_1^2(a\zeta)}\left\{1 + \frac{k_0 r_0}{a\zeta}\operatorname{sech}^2[k_1(r_1 - r_0)]\right\}, \tag{20}$$

$$\begin{aligned} r_{\rm v} =& \frac{k_0^2 + k_1^2}{k_0 k_1^2(a\zeta)}\frac{r_1}{a}\left\{1 - \frac{1}{k_1 r_1}\tanh[k_1(r_1 - r_0)]\right\} \\ &+ \frac{1}{k_1^2 a} - \frac{r_1^3}{3a^2}. \end{aligned} \tag{21}$$

At resonance where a diverges (the combination of $a\zeta$ stays finite), the vanishing part $r_{\rm v}$ is zero, and the expression for r_e reduces to

$$r_{e0} = r_1 - \frac{k_0^2+k_1^2}{k_0^2 k_1}\frac{\tanh[k_1(r_1-r_0)]}{1-\tanh^2[k_1(r_1-r_0)]} \times \{1 + k_1 r_0 \tanh[k_1(r_1-r_0)]\}, \qquad (22)$$

or equivalently

$$r_{e0} = r_1 + \frac{k_0^2+k_1^2}{k_0}\frac{\tan(k_0r_0)-k_0r_0}{k_1^2\tan^2(k_0r_0)-k_0^2}. \qquad (23)$$

In addition, the condition for resonance ($\zeta = 0$) becomes $\tan(k_0r_0) < -k_0/k_1$. We can see, from Eq. (22), that the effective range r_{e0} at resonance is smaller than r_1 since $0 \leq \tanh[k_1(r_1-r_0)] < 1$. In the weak barrier limit, $\xi \equiv k_1(r_1-r_0) \ll 1$, the effective range at resonance can be written as

$$r_{e0} \simeq r_0 - \frac{k_1}{k_0^2}\xi + O(\xi^2). \qquad (24)$$

Thus adding a weak barrier to a square-well potential with the range r_0 yields smaller effective range at resonance than that for the original square-well potential $r_{e0} = r_0$. The decrease of r_{e0} means an enhancement of the amplitude in the potential region, which can be understood as an effect of blocking probability leakage due to the additional barrier.

B. Effective range and scattering properties

To begin with, we illustrate the physical meaning of the effective range explicitly. In Fig. 2, we plot the wave functions for $|a| \to \infty$ in the cases of (a) positive and (b) negative effective range for the same values of k, r_0, k_1, and different r_1. It is clearly seen that the resonance wave function for a negative effective range has a large amplitude in the potential range as mentioned before. Even in the case of Fig. 2 (a), a small bump can be observed close to the edge of the potential, which means a small decrease of the effective range compared to the square-well potential shown by Eq. (24). At $r_e = 0$, the mean value of $|\psi|^2$ for $r < r_1$ is unity, $r_1^{-1}\int_0^{r_1}|\psi|^2 dr = 1$, thus $\int_0^{r_1}(1-\psi^2)dr = 0$ as given by Eq. (10).

We now discuss the scattering properties of the square-well, square-barrier potential in detail. In Figs. 3 and 4, we plot the parameter regions in which the effective range is negative and the absolute value of the scattering length is large close to resonance. Figure 3 shows the dependence of these regions on the barrier width $r_1 - r_0$ at fixed r_0 and k_1. As $r_1 - r_0$ increases, the width of the dark gray regions becomes smaller, which means the resonance becomes narrower. The effective range at resonance decreases from r_0, which is for the square-well potential, to $-\infty$ with increasing $r_1 - r_0$. This can also be seen from Eq. (22) where the absolute value of the second term increases monotonically from zero to infinity as $r_1 - r_0$ increases with r_0, k_0, and k_1 fixed. Figure 4 shows the dependence of the above regions on the barrier height k_1 at fixed r_0 and r_1. Similarly to the above case, as k_1 increases, the resonance becomes narrower and r_e at resonance decreases from r_0 to $-\infty$ monotonically. This continuous decrease can be proved analytically by calculating the derivative of Eq. (23) with respect to k_1 and by taking the necessary condition for resonance, $\tan(k_0r_0) < -k_0/k_1$, into account. From both Figs. 3 and 4, we see that the resonance for the deeper potential well (larger k_0) is narrower.

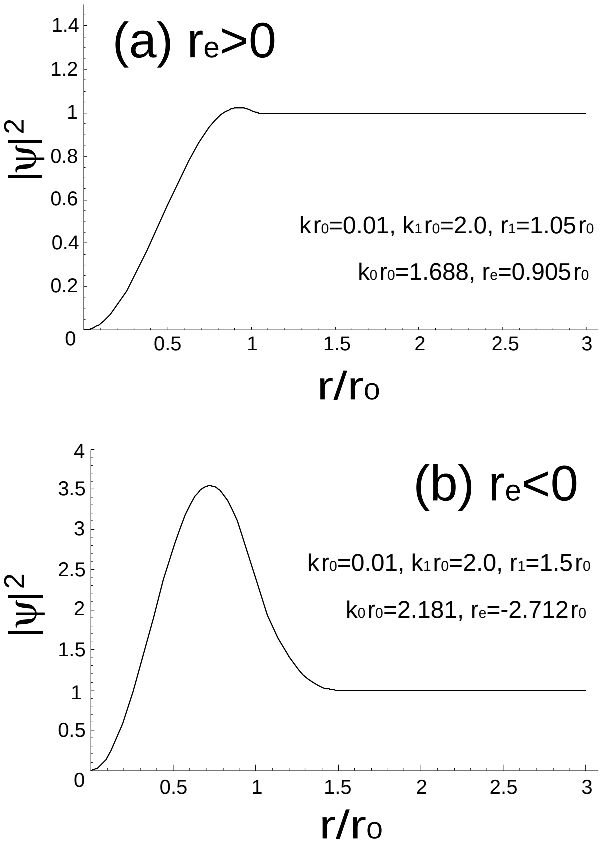

Figure 2: Resonance wave functions for (a) positive and (b) negative effective range. In the both cases, we take $kr_0 = 0.01$ and $k_1r_0 = 2.0$, and ψ is normalized so that $\psi(r) = \sin(kr+\delta)$ for $r > r_1$.

Let us finally mention the behavior of the scattering length and the effective range away from resonance. In Figs. 5 and 6, we plot these quantities as functions of the width $r_1 - r_0$ and the height parameter k_1 of the barrier, respectively. The scattering length, which almost corresponds to the background one, increases linearly with r_1 for large barrier widths (see Fig. 5):

$$a \simeq r_1 - \frac{1}{k_1}. \qquad (25)$$

However, this quantity does not change so much when

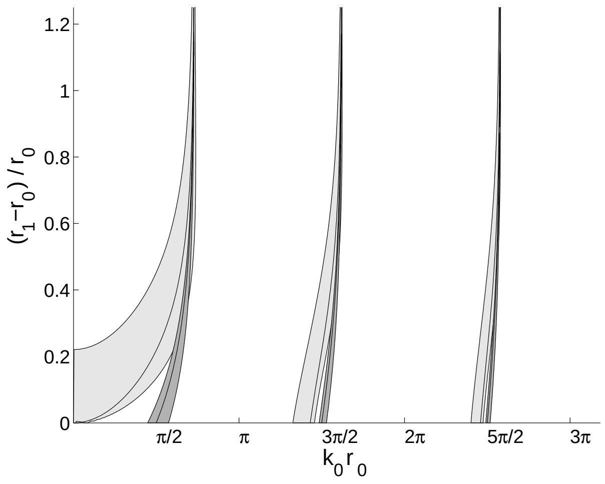

Figure 3: Parameter regions of k_0 and $r_1 - r_0$ at fixed $k_1 r_0 = 2$ for negative effective range (light gray region) and for resonance (dark gray region). Here the resonance region is defined by $|r_0/a| < 0.3$; $r_0/a = -0.3$ on the left boundary of the dark gray area and $r_0/a = 0.3$ on that of the right one. The line plotted in the dark gray region corresponds to $1/|a| = 0$. The boundary of the light gray region corresponds to $r_e = 0$, and the curve in this region shows $r_e = -\infty$.

k_1 increases. It starts from a value comparable to r_1 at $k_1 = 0$ and converges to r_1 as $k_1 \to \infty$ (see Fig. 6). Whether it approaches r_1 from above or below depends on the value of $k_0 r_0$. The behavior of the effective range is similar to that of the scattering length. It increases linearly with r_1 at large $r_1 - r_0$ (Fig. 5):

$$r_e \sim \frac{2}{3} r_1, \tag{26}$$

and, with increasing k_1, it remains of order r_1 and converges to $2r_1/3$ as $k_1 \to \infty$ (Fig. 6).

IV. NON-UNIVERSAL ZERO TEMPERATURE BCS-BEC CROSSOVER

In the present section we examine the BCS-BEC crossover problem for a gas of equal numbers $N/2$ in two different internal states interacting through the square-well, square-barrier potential within an effective single-channel model.

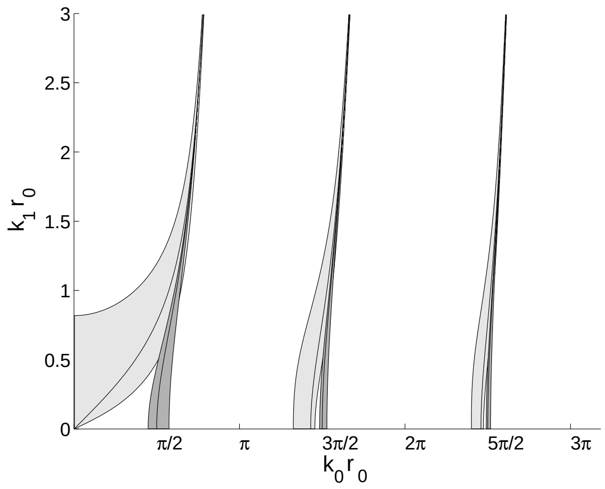

Figure 4: The same as Fig. 3 for parameter regions of k_0 and k_1 at fixed $r_1 = 2r_0$ for negative effective range (light gray region) and for resonance (dark gray region).

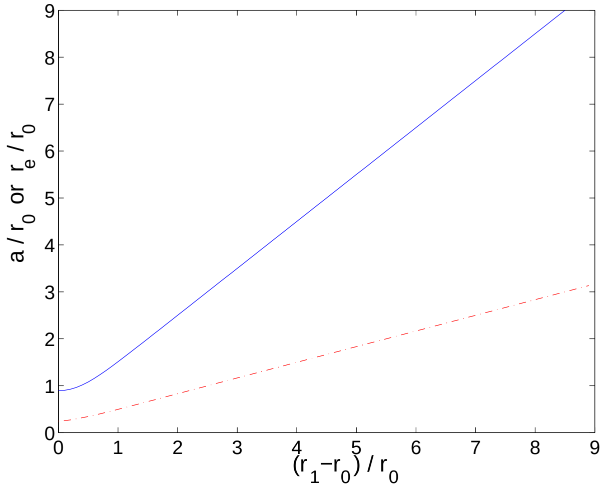

Figure 5: (Color online) The scattering length a (solid line) and the effective range r_e (dash-dotted line) as functions of the barrier width $r_1 - r_0$. We take $k_0 r_0 = 2$ and $k_1 r_0 = 2$.

A. Basic formalism

The Hamiltonian H for the two-component Fermi gas is

$$\begin{aligned} H = & \sum_{\mathbf{k},\sigma} \varepsilon_{\mathbf{k}} a^{\dagger}_{\mathbf{k}\sigma} a_{\mathbf{k}\sigma} \\ & + \frac{1}{\mathcal{V}} \sum_{\mathbf{k}\mathbf{k}'} U_{\mathbf{k}\mathbf{k}'} a^{\dagger}_{\mathbf{k}\uparrow} a^{\dagger}_{-\mathbf{k}\downarrow} a_{-\mathbf{k}'\downarrow} a_{\mathbf{k}\uparrow}, \end{aligned} \tag{27}$$

where $a^{\dagger}_{\mathbf{k}\sigma}, a_{\mathbf{k}\sigma}$ are the creation and annihilation operators, respectively, of atoms with wave vector $\mathbf{k}$, and pseudospin index, $\sigma = \uparrow$ or $\downarrow$. The single particle kinetic

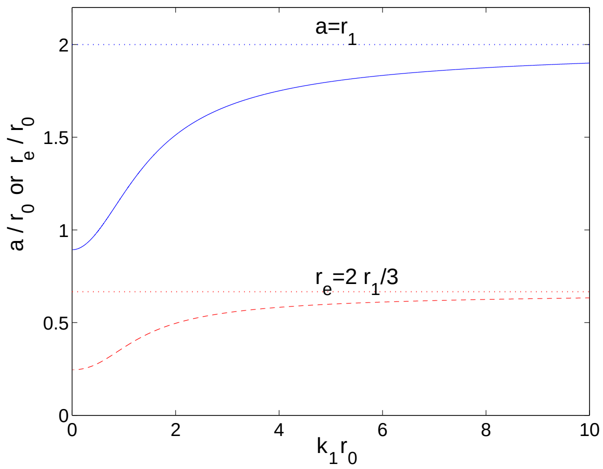

Figure 6: (Color online) The scattering length a (solid line) and the effective range r_e (dashed line) as functions of the barrier height k_1. The dotted lines show the asymptotic values of these quantities. We take $k_0r_0 = 2$ and $r_1 = 2r_0$.

energy is $\varepsilon_{\mathbf{k}} = \hbar^2\mathbf{k}^2/(2m)$, and the inter-atomic interaction in momentum space is $U_{\mathbf{k}\mathbf{k}'}$. The zero temperature BCS-BEC crossover problem is here numerically studied along the lines of Refs. [8, 20, 21, 22, 27] based on the BCS variational state

$$|\Psi_{\rm BCS}\rangle = \Pi_{\mathbf{k}}\left(u_{\mathbf{k}} + v_{\mathbf{k}}a^\dagger_{\mathbf{k}\uparrow}a^\dagger_{-\mathbf{k}\downarrow}\right)|\Psi_0\rangle, \tag{28}$$

where $|\Psi_0\rangle$ is the vacuum state, and $u_{\mathbf{k}}$ and $v_{\mathbf{k}}$ are the variational parameters normalized according to the condition $|u_{\mathbf{k}}|^2 + |v_{\mathbf{k}}|^2 = 1$. The energy of the BCS state $E(u_{\mathbf{k}}, v_{\mathbf{k}}) = \langle\Psi_{\rm BCS}|H|\Psi_{\rm BCS}\rangle$ is to be minimized with respect to the variational parameters $u_{\mathbf{k}}$ and $v_{\mathbf{k}}$, subject to the normalization condition and the requirement that the mean particle number $N(u_{\mathbf{k}}, v_{\mathbf{k}}) = \sum_{\mathbf{k},\sigma}\langle\Psi_{\rm BCS}|a^\dagger_{\mathbf{k}\sigma}a_{\mathbf{k}\sigma}|\Psi_{\rm BCS}\rangle = 2\sum_{\mathbf{k}}|v_{\mathbf{k}}|^2$ should be fixed. By introducing the Lagrange multipliers $E_{\mathbf{k}}$ and μ to ensure normalization and number conservation, the stationary condition $\delta[E - \mu N - \sum_{\mathbf{k}} E_{\mathbf{k}}(|u_{\mathbf{k}}|^2 + |v_{\mathbf{k}}|^2)]/\delta(u_{\mathbf{k}}, v_{\mathbf{k}}) = \mathbf{0}$ yields $\xi_{\mathbf{k}}u_{\mathbf{k}} + \Delta_{\mathbf{k}}v_{\mathbf{k}} = E_{\mathbf{k}}u_{\mathbf{k}}$ and $u_{\mathbf{k}}\Delta^*_{\mathbf{k}} - \xi_{\mathbf{k}}v_{\mathbf{k}} = E_{\mathbf{k}}v_{\mathbf{k}}$, where $\xi_{\mathbf{k}} \equiv \hbar^2k^2/(2m) - \mu$. Here, the momentum dependent gap function is defined as $\Delta_{\mathbf{k}} = \sum_{\mathbf{k}'} U_{\mathbf{k}\mathbf{k}'}u_{\mathbf{k}'}v^*_{\mathbf{k}'}$. By solving the above equations, one determines the usual quasi-particle energy $E_{\mathbf{k}} = (\xi^2_{\mathbf{k}} + \Delta^2_{\mathbf{k}})^{1/2}$ and the coherence factors $|u_{\mathbf{k}}|^2 = (1 + \xi_{\mathbf{k}}/E_{\mathbf{k}})/2$ and $|v_{\mathbf{k}}|^2 = (1 - \xi_{\mathbf{k}}/E_{\mathbf{k}})/2$. Inserting the expression for $u_{\mathbf{k}}v^*_{\mathbf{k}} = \Delta_{\mathbf{k}}/(2E_{\mathbf{k}})$ into the definition of the gap yields the gap equation:

$$\Delta_{\mathbf{k}} = -\frac{1}{\mathcal{V}}\sum_{\mathbf{k}'} U_{\mathbf{k}\mathbf{k}'}\frac{\Delta_{\mathbf{k}'}}{2E_{\mathbf{k}'}}. \tag{29}$$

This is to be solved self-consistently together with the equation for the atomic number density

$$n = \frac{1}{\mathcal{V}}\sum_{\mathbf{k}}\left(1 - \frac{\xi_{\mathbf{k}}}{E_{\mathbf{k}}}\right). \tag{30}$$

At fixed density $n = k_{\rm F}^3/(3\pi^2)$, where $k_{\rm F}$ is the Fermi momentum for the non-interacting gas, Eq. (30) determines the chemical potential, μ. For the contact interaction, the regularized homogeneous BCS-BEC crossover problem [7, 8] is analytically solvable [28, 29, 30] and results in the zero range (Leggett) reference curves in Figs. 7, 9, 11, 12, and 13.

The partial wave decomposition of the interaction potential is

$$\begin{aligned} U_{\mathbf{k}\mathbf{k}'} &= \int d^3r\; e^{i(\mathbf{k}-\mathbf{k}')\cdot\mathbf{r}}\; U(\mathbf{r}) \\ &= \sum_{\ell=0}^{\infty}(2\ell+1)4\pi U_\ell(k,k')P_\ell(\hat{k}\cdot\hat{k}'), \end{aligned} \tag{31}$$

with

$$U_\ell(k,k') = \int_0^\infty dr\; r^2 j_\ell(kr)U(r)j_\ell(k'r). \tag{32}$$

Here $j_\ell(x) = \sqrt{\pi/(2x)}J_{\ell+1/2}(x)$ is the ℓ'th spherical Bessel function defined from the ν'th ordinary Bessel function of the first kind, $J_\nu(x)$, and P_ℓ is the ℓ'th Legendre function with $\hat{k}\cdot\hat{k}' = \cos\theta$, θ being the angle between the unit vectors $\hat{k}$ and $\hat{k}'$. We also used the addition formula $(2\ell+1)P_\ell(\hat{k}\cdot\hat{k}') = 4\pi\sum_{m=-\ell}^{\ell}Y^*_{\ell m}(\hat{k})Y_{\ell m}(\hat{k}')$ for the spherical harmonic functions $Y_{\ell m}(\hat{k})$. The momentum dependent gap can be decomposed in the same way as

$$\Delta_{\mathbf{k}} = \sum_{\ell=0}^{\infty}\sum_{m=-\ell}^{m}\Delta_{\ell m}j_\ell(k)Y_{\ell m}(\hat{k}), \tag{33}$$

where the $\Delta_{\ell m}$'s are the angular weight coefficients. With the assumption that the main low energy contribution to the gap is of s-wave ($\ell = 0$) character, the gap equation reduces to

$$\Delta(k) = -\frac{1}{\pi}\int dk'\; k'^2\frac{U_0(k,k')\Delta(k')}{\sqrt{\xi^2_{k'} + \Delta^2(k')}}, \tag{34}$$

where the s-wave part of the potential is

$$\begin{aligned} U_0(k,k') = &\int_0^\infty dr\; r^2 j_0(kr)U(r)j_0(k'r) \\ = &\frac{U_0+U_1}{2kk'}\left[\frac{\sin\left(|k+k'|r_0\right)}{|k+k'|} - \frac{\sin\left(|k-k'|r_0\right)}{|k-k'|}\right] \\ &- \frac{U_1}{2kk'}\left[\frac{\sin\left(|k+k'|r_1\right)}{|k+k'|} - \frac{\sin\left(|k-k'|r_1\right)}{|k-k'|}\right]. \end{aligned} \tag{35}$$

B. Solution of the crossover equations

The crossover equations consist of Eq. (30) and Eq. (34) together with the expression (35) for the momentum dependent interaction. We notice that, for a finite range interaction potential vanishing beyond a scale r_1, all momentum integrals are cutoff typically at the scale of $1/r_1$ and therefore remain ultraviolet convergent. Here, r_1 characterizes the range of the interatomic interactions. In the context of ultracold atoms, r_1 can be taken to be the characteristic scale of the van der Waals interaction. We shall consider a system at fixed density and will study the properties of the system as the potential is changed by varying the well depth, the barrier height or the barrier width. Finally, in order to describe the crossover in terms of physically relevant two-body quantities, we parametrically plot quantities versus the scattering length a obtained from Eq. (17) and the effective range r_e obtained from Eq. (19) as functions of the model parameters.

Below, we briefly describe our numerical procedure used to solve the crossover equations. By discretizing the momenta on a finite grid, the gap equation (34) and the number density equation (30) were solved iteratively for the given density. The spacing of the momentum grid, Δk, was chosen to provide sufficient sampling on the scale of $k_{\rm F} \sim n^{1/3}$. The maximum momentum $k_{\rm max}$ was chosen to be much larger than the scales of the internal range of the potential r_0^{-1} and r_1^{-1}. All results shown below are calculated with $\Delta k = k_{\rm F}/15$ and $k_{\rm max} = 2500\Delta k$ (this corresponds to $k_{\rm max} \simeq 50 r_0^{-1}$ for the model parameters employed). The system was driven from the BEC to the BCS limit and the initial guess for the k-dependent gap function $\Delta(k)$ was determined from the Fourier transform of the real space wave function determined in Section III. The equations were solved by iteration, and the process was continued until the difference in μ between successive iterations was less than one part in 10^6. The results were checked to be insensitive to further increase of grid size, $k_{\rm max}$, and decrease of grid spacing, Δk.

We consider the case of driving the BCS-BEC crossover by varying the potential well parameter k_0 around its critical value k_{0c} at which the scattering length diverges. Both the scattering length and the effective range depend on k_0 and therefore r_e/r_0 depends on $(k_{\rm F}a)^{-1}$ through the parameter k_0. Figure 7 contains parametric plots of the effective range versus the scattering length for different values of the barrier width $r_1 - r_0$. As we are interested in the scattering properties of the model and not in the particular values of the model parameters, it is more natural to show the r_e curves in terms of the effective range r_{e0} at $(k_{\rm F}a)^{-1} = 0$. The barrier widths used in the calculations, $(r_1 - r_0)/r_0 = 0.1, 0.25, 0.30, 0.35$, and 0.40, correspond to effective ranges $r_{e0}/r_0 \approx 0.78, 0.12, -0.23, -0.66$, and -1.20. The remaining parameter k_1 was chosen to be $k_1 r_0 = 2.0$, and the density was chosen as $n = 0.001 r_0^{-3}$, i.e., $k_{\rm F} r_0 \simeq 0.31$. For relative large and positive r_{e0}, the effective range is only weakly dependent on the coupling constant in the crossover region as evidenced by the solid line in Fig. 7. As r_{e0} decreases, the effective range develops a strong dependence on the inverse coupling constant. We note that similar results for r_e presented in Fig. 7 could have been obtained by changing the barrier height instead. Such a degeneracy is to be expected for potentials with many model parameters since the mapping of the model parameters to the effective low energy parameters is a many-to-two mapping. In the Eagles-Leggett model, only the scattering length appears and it is therefore interpreted as the $r_{e0} = 0$ case with $r_e = 0$ for all couplings.

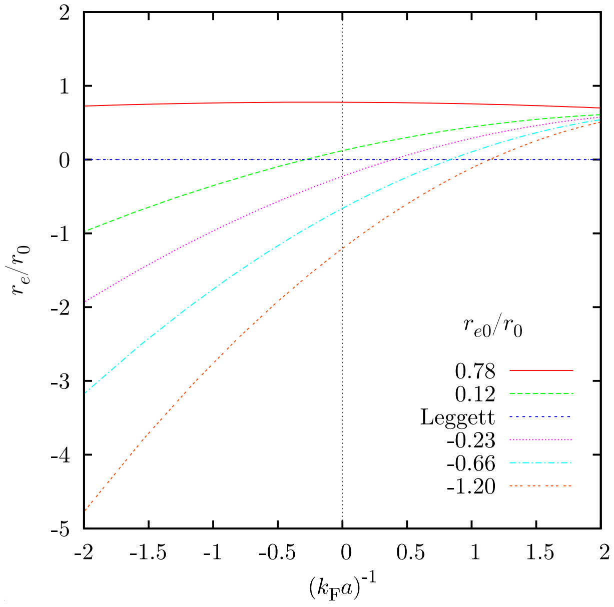

Figure 7: (Color online) The effective range r_e/r_0 as a function of the dimensionless constant $(k_F a)^{-1}$. The density is set to be $k_{\rm F} r_0 \simeq 0.31$.

C. Energy gap

We first examine the effective range dependence of the gap parameter $\Delta(k)$. In panels (a)-(c) of Fig. 8, $\Delta(k)/E_{\rm F}$ obtained from the crossover equations is displayed for several values of r_{e0}, here $E_{\rm F} \equiv \hbar^2 k_{\rm F}/2m$ is the Fermi energy for the non-interacting gas. The solid curves in panels (a)-(c) show the evolution of $\Delta(k)$ in the near BCS limit. In this limit, the gap has a maximum at $k = 0$ for relatively large and positive r_{e0} as displayed in panel (a). As r_{e0} decreases, the maximum flattens and the sign of the curvature at $k = 0$ changes from negative to positive as can be seen by comparing the solid curves in panels (a) and (b). For negative r_{e0}, the gap has a local minimum at $k = 0$ and the maximum of the gap moves to a higher k [see the solid curve in panel (c)].

The energy gap in the ground state is the minimum of the quasiparticle dispersion $E_{\mathbf{k}}$ for all $\mathbf{k}$ [8] and, for a Fermi gas with contact interactions, the gap $\Delta_{\mathbf{k}} = \Delta$ is momentum independent. For a positive μ, the energy $E_{\mathbf{k}} = (\xi_{\mathbf{k}}^2 + \Delta^2)^{1/2}$ is minimized at $\hbar^2 k^2/2m = \mu$ with the value $E_{\rm min} = |\Delta|$. On the other hand, for a negative μ, the energy minimum $E_{\rm min} = (\mu^2 + \Delta^2)^{1/2}$ is attained

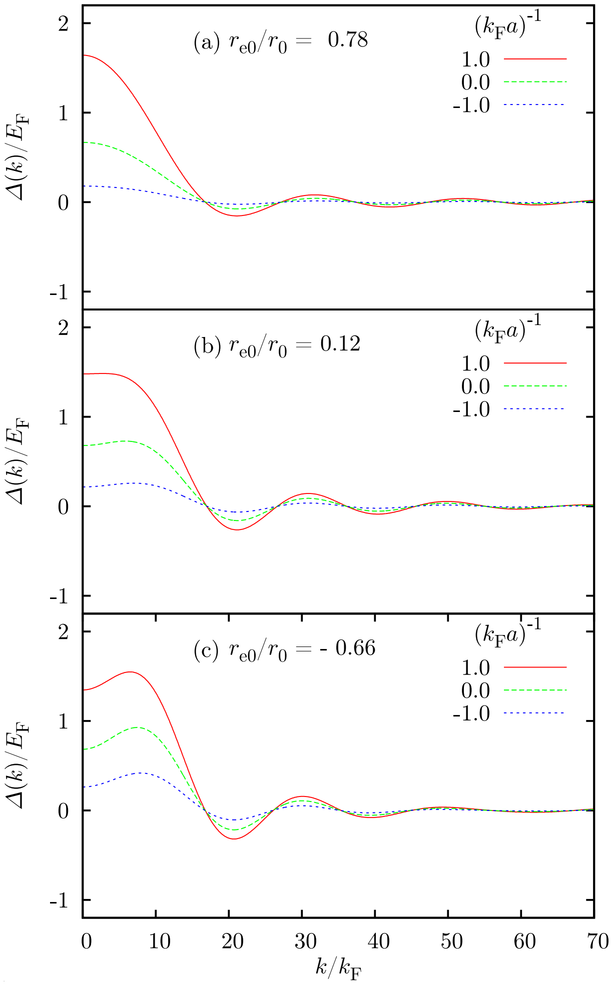

Figure 8: (Color online) The solution of the gap equation for the values $(k_Fa)^{-1} = -1, 0,$ and 1 of the inverse coupling constant is presented for several values of the effective range r_{e0} in the unitarity limit. For positive effective range (a), the zero momentum gap is a local maximum. Close to zero effective range, the maximum turns into a plateau with a vanishing momentum gradient. In (c), the zero momentum gap is turned into a local minimum for all values of the inverse coupling. The density is set to be $k_F r_0 \simeq 0.31$.

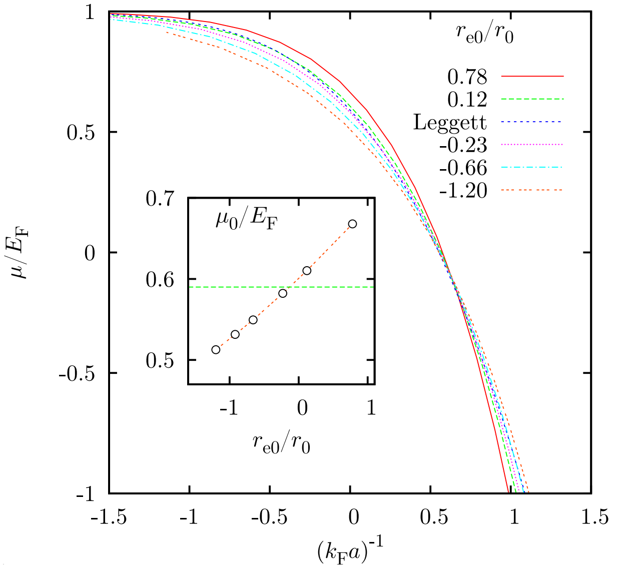

Figure 9: (Color online) The chemical potential μ/E_F versus $(k_Fa)^{-1}$ is plotted for changing the depth of the potential well [32]. Each curve is labeled by the value of the dimensionless effective range r_{e0}/r_0 in the unitarity limit. As the effective range becomes negative, the finite range correction to the universal chemical potential changes its sign. In the inset, we have plotted the chemical potential μ_0 in the unitarity limit, $(k_Fa)^{-1} = 0$, as a function of the unitary effective range r_{e0}. The universal result $\mu_0/E_F \approx 0.59$ obtained by Leggett [8] is marked with the horizontal dashed line. The density is set to be $k_F r_0 \simeq 0.31$.

at $k = 0$. Therefore, as the interaction is decreased from the BEC limit to the BCS one, the $k_{\min}$ value, where $E_{\mathbf{k}}$ has its minimum, shifts from 0 to $\sqrt{2m\mu/\hbar^2}$ at $\mu = 0$ to $k_{\min} = k_F$ in the BCS limit. Due to the interaction-induced shift in the position of $k_{\min}$, the functional behavior of $E_{\mathbf{k}}$ is also directly reflected in the pair wave function $\psi(k) = \Delta/(2E_{\mathbf{k}})$ which appears directly in the gap equation, and also in a number of derived quantities such as the healing length and condensate fraction. In the BEC limit, where the gap equation reduces to the equation for two bound particles, $\psi(k)$ represents the internal wave function of the pair. The $1/E_{\mathbf{k}}$ dependence implies a maximum of $\psi(k)$ at $k = 0$ for $\mu < 0$ (the BEC case) and at $\sqrt{2m\mu}/\hbar$ for $\mu > 0$, the BCS case (see also [20]).

Next we consider the functional behavior in the general case of a momentum dependent gap $\Delta_{\mathbf{k}}$. We assume that the Fermi gas is so dilute that the range of the potential is much shorter than the interatomic spacing, i.e., $r_0, r_1 \ll k_F^{-1}$. The momentum dependent gap varies on the scale of $1/r_0$ which is large compared with k_F, and therefore the behaviors described above for a constant gap are expected to be rather general [31].

D. Chemical potential

Next we discuss the influence of the nonzero effective range on the chemical potential. Figure 9 contains a plot of the chemical potential as a function of $(k_Fa)^{-1}$ for several values of r_{e0}. At a sufficiently low value of r_{e0}, the chemical potential approaches the universal result (short blue dashes denoted by "Leggett") as obtained from the zero-range model. By an additional variation of the barrier parameter, the effective range r_{e0}/r_0 is varied from a positive value 0.78 (solid line) to -1.20 (dotted line). The plots of the chemical potential for different values of r_{e0} are all seen to cross at $(k_Fa)^{-1} \approx 0.55$, where μ is close to zero. The inset in Fig. 9 contains a plot of the chemical potential μ_0 at $k_F|a| \to \infty$ as a function of the effective range, which clearly shows the correction due to the effective range. The horizontal dashed line of $\mu_0/E_{\rm F} \approx 0.59$ corresponds to μ_0 for a contact potential, and the crossing of this line at $r_{e0} \approx 0$ also validates our approach to discuss non-universal corrections by use of a finite-range model potential. For positive r_{e0}, the chemical potential for $k_{\rm F}|a| \to \infty$ is enhanced with respect to the zero range case as was also observed in Ref. [20] based on the Gaussian potential. On the other hand for a negative r_{e0} the chemical potential is reduced compared to the curve for a contact potential. These non-universal corrections become small with decreasing density. We have observed that, for a lower density of $n = 0.0001 r_0^{-3}$, i.e., $k_{\rm F} r_0 \simeq 0.14$, deviations from the Leggett curve in the region $-1 \lesssim (k_{\rm F}a)^{-1} \lesssim 1$ are about a factor of two smaller than those in Fig. 9.

By matching the scattering properties of single- and two-channel models on resonance, it is found that $4\pi\hbar^2 a/m = -g^2/\nu$ and $r_{e0} = -8\pi\hbar^4/(mg^2)$, where g is the atom-molecule coupling and ν is the detuning in the two-channel boson-fermion model [33]. Because of r_{e0} is negative in this model, for $(k_{\rm F}a)^{-1} \simeq 0$, the above non-universal reduction of the chemical potential is expected in less wide to narrow Feshbach resonances [21, 22]. It is also noted that this reduction close to a narrower resonance cannot be achieved with a monotonic attractive potential (which all have $r_{e0} > 0$) and therefore constrains the model potential when modelling atom gases.

In Fig. 10, we compare the chemical potential and the binding energy $E_{\rm b}$ of the two-body bound state of the same square-well, square-barrier potential. For $a \gg r_0, r_1$, the binding energy is well approximated by using only a and r_e as $E_{\rm b} \simeq (\hbar^2/ma^2)(1 + r_e/a)$ ($E_{\rm b}$ is defined to be positive), and thus the negative effective range reduces the binding energy close to threshold. For $a \lesssim r_0, r_1$, since the extension of the wave function of the bound state is comparable to the range of the potential, $E_{\rm b}$ depends strongly on its specific shape. Therefore, $E_{\rm b}$ for a potential with a larger negative r_{e0}, which has a stronger barrier [i.e., larger $\xi = k_1(r_1 - r_0)$], is smaller at $(k_{\rm F}a)^{-1} \gg 1$. We can also see that the chemical potential consistently behaves as $\mu \to -E_{\rm b}/2$ in this limit.

E. Consequences of the nonzero effective range in non-universal resonances

Most experiments on the BCS-BEC crossover done so far have been performed with broad resonances. According to an estimate in [22], $k_{\rm F} r_e \sim 0.01$ and $r_e/r_0 \lesssim 1$ [37] in the experiment by Regal *et al.* [1], and $k_{\rm F} r_e \sim 10^{-4}$ and $r_e/r_0 \sim 0.1$ in the experiment by Zwierlein *et al.* [2]. Due to the small values of $k_{\rm F} r_e$, the effective range has an imperceptible effect in these experiments. However, it is essential to study narrower resonances, in which effective range corrections are significant, for understanding strongly interacting Fermi gases more deeply. Therefore, consequences of the nonzero effective range, especially for negative cases, in future experiments on narrow resonances are worth discussing. In the remaining part of this paper, we study effective range corrections for uniform systems on the following four measurable quantities. zero momentum gap, momentum distribution, and condensate fraction.

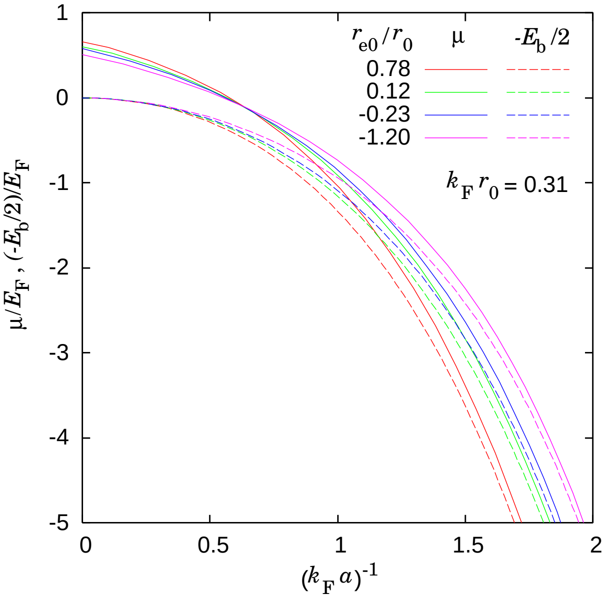

Figure 10: (Color online) Comparison between the chemical potential (solid lines) and the binding energy $E_{\rm b}$ of the two-body bound state (dashed lines) for several values of the effective range $r_{e0}/r_0 = 0.78$ (red), 0.12 (green), -0.23 (blue), and -1.2 (magenta). The density is set to be $k_{\rm F} r_0 \simeq 0.31$.

1. *Zero momentum gap*

In Fig. 11 the zero momentum gap $\Delta(0)$ is plotted as a function of $(k_{\rm F}a)^{-1}$. All curves cross at almost the same point near $(k_{\rm F}a)^{-1} = 0$ and thus the zero momentum gap shows little dependence on r_{e0} close to resonance. In the BCS region $[(k_{\rm F}a)^{-1} < 0]$, however, the effective range corrections can be significant and $\Delta(0)$ is enhanced for large and negative r_{e0}. A larger negative value of r_{e0}, which is yielded by a stronger barrier [larger $\xi = k_1(r_1 - r_0)$] in the present single-channel model, corresponds to a weaker atom-molecule coupling g in a two-channel model. Thus, in this case, BCS pairing is more favorable on the BCS side and the gap is enhanced. This result can be also understood in terms of the effective range expansion introducing the effective scattering length $a_e(k)$:

$$\frac{1}{a_e(k)} \equiv \frac{1}{a} - \frac{1}{2} r_e k^2. \tag{36}$$

For negative a and r_e, the absolute value of the effective scattering length $|a_e|$ is larger than $|a|$; i.e., the effective range correction due to a negative r_e yields a stronger

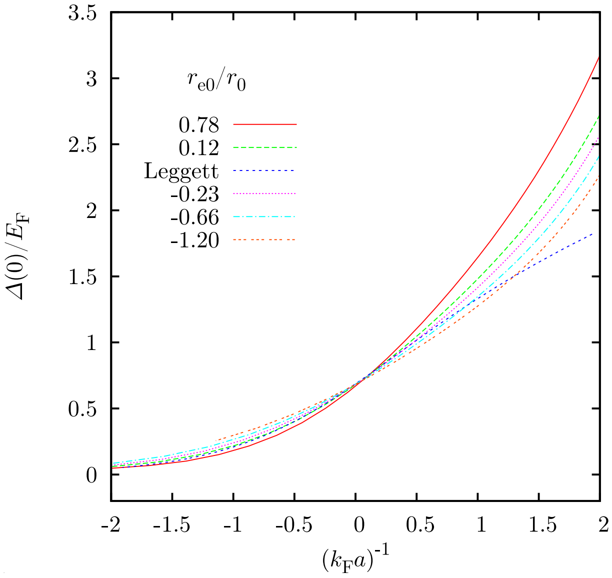

Figure 11: (Color online) The zero temperature gap $\Delta(0)/E_{\rm F}$ at $k = 0$ is plotted as a function of the inverse coupling constant $(k_{\rm F}a)^{-1}$ for several values of the effective range $r_{\rm e0}/r_0$. The density is set to be $k_{\rm F}r_0 \simeq 0.31$.

attractive interaction on the BCS side, which leads to a larger BCS gap. Using the effective scattering length, we may write $\Delta(0)/E_{\rm F} \approx (8/e^2)e^{-2\{k_{\rm F}a_e(k_{\rm F})\}^{-1}/\pi} = (8/e^2)e^{\{2(k_{\rm F}a)^{-1}-k_{\rm F}r_e\}/\pi}$ in the BCS limit, which converges toward $(8/e^2)e^{-2(k_{\rm F}a)^{-1}/\pi}$ in the far BCS limit.

In the far BEC regime $[(k_{\rm F}a)^{-1} \gg 1]$, where the molecules are deeply bound, $\Delta(0)$ also strongly depends on the specific properties of the potential, as has been seen for the chemical potential, and therefore it deviates from the zero range result. The suppression of $\Delta(0)$ for a large, negative r_{e0} compared to that for a small negative or positive r_{e0} can be attributed to the stronger repulsive barrier in the former case, which acts to destroy the pair in this regime. We have also confirmed that, with decreasing density, $\Delta(0)$ for each value of r_{e0} approaches the one for a contact potential. For a lower density of $n = 0.0001r_0^{-3}$, the effective range corrections in the region of $-1 \lesssim (k_{\rm F}a)^{-1} \lesssim 1$ are about a factor of two smaller than those in Fig. 11, as in the case of the chemical potential [38].

2. *Momentum distribution*

The momentum distribution $n_k/2 = |v_k|^2/\mathcal{V}$ of fermion atoms (for spin-up or spin-down) is shown in Fig. 12, where n_k being $2|v_k|^2/\mathcal{V}$. Here we plot $n_k/2$ for $(k_{\rm F}a)^{-1} = -1, 0,$ and 1 for the same parameter sets as in Fig. 8. In the near to far BEC limits of $(k_{\rm F}a) \gtrsim 1$, all curves for different r_{e0} almost coincide with the one for the contact potential. However, from the unitarity regime $(k_{\rm F}a)^{-1} \sim 0$ to the near BCS limit $(k_{\rm F}a)^{-1} \sim -1$, we observe significant effective range corrections. The results for $(k_{\rm F}a)^{-1} = -1$ and 0 in this figure show that corrections due to the negative effective range suppress $n_{k=0}$ and broaden the momentum distribution. As discussed before, a large, negative r_{e0}, which corresponds to a weak atom-molecule coupling, favors the BCS state on the BCS side. Therefore the Fermi surface is smeared and n_k is broadened in this case.

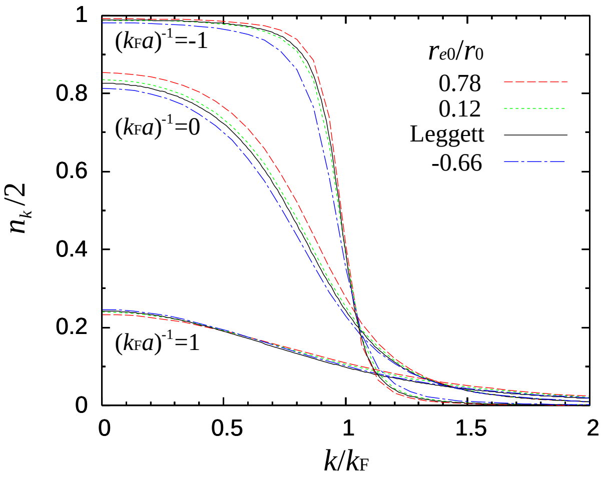

Figure 12: (Color online) The momentum distribution $n_k/2$ of fermion atoms for $(k_{\rm F}a)^{-1} = -1, 0,$ and 1 is presented for several values of of the effective range r_{e0} in the unitarity limit. The density is set to be $k_{\rm F}r_0 \simeq 0.31$.

3. *Condensate fraction*

We consider the influence of the effective range on the condensate fraction in the BCS-BEC crossover. In a Fermi gas, the appearance of superfluid order is related to the appearance of off-diagonal long range order as found in the two-body density matrix. Following [34, 35, 36], we calculate the number of the condensed fermion pairs as $N_0 = \sum_{\mathbf{k}} |u_{\mathbf{k}}v_{\mathbf{k}}|^2$ and examine the influence of the nonzero effective range.

Figure 13 contains a plot of the normalized condensate fraction $N_0/(N/2) = 2N_0/N$ of a Fermi gas as a function of the inverse coupling for the same parameter sets as those used in Figs. 9 and 11. Within the mean-field approximation, the normalized molecular condensate fraction converges to unity in the BEC limit independent of the detailed nature of the potential. On the other hand, when the binding energy is decreased, the dimers dissociate more easily and the condensate fraction correspondingly decreases and eventually vanishes in the BCS limit. For a large and negative value of r_{e0}, the dissociation is suppressed due to the weak atom-molecule coupling, and thus the condensate fraction is enhanced as shown in this figure.

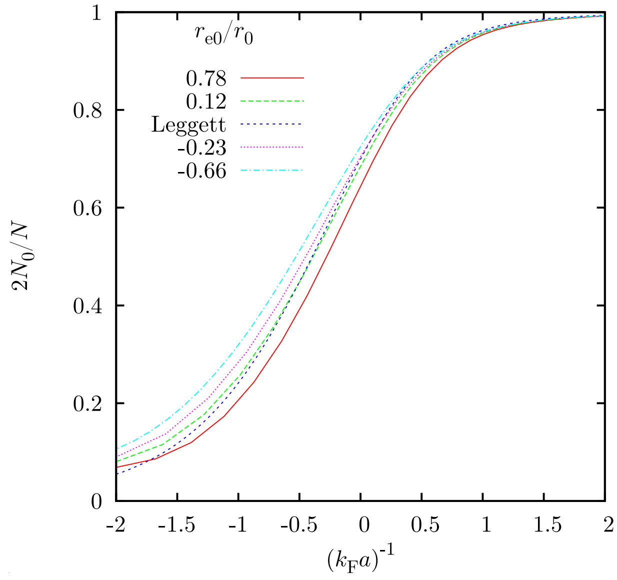

Figure 13: (Color online) The normalized zero temperature condensate fraction $N_0/(N/2)$ as a function of the inverse coupling constant $(k_F a)^{-1}$ for several values of the effective range r_{e0}/r_0. The density is set to be $k_F r_0 \simeq 0.31$.

V. SUMMARY AND CONCLUSION

We have presented a detailed study of the two-body bound state and scattering properties of a simple solvable model potential with a barrier to model the narrow resonance phenomena in the BCS-BEC crossover in atomic Fermi gases. We paid particular attention to the effect of the nonzero effective range and its sign as the inverse scattering length was tuned from large negative values to large positive ones. The advantage of our simple single-channel potential model is that it explicitly displays the relation between the potential resonance phenomena and the appearance of negative effective range, which is predicted by two-channel models.

First, we studied the two-particle scattering problem with the square-well, square-barrier potential, and have clearly demonstrated the physical meaning of the negative effective range. The effective range at resonance was carefully analyzed and the analytical expression for the weak barrier case was also presented. This expression shows that adding a barrier to a square-well potential yields smaller values of the effective range.

We then applied this potential to the BCS-BEC crossover phenomena within an effective single-channel potential model. By solving the crossover equations self-consistently, we studied the effects of both the positive and negative effective range within a unified framework. We have observed that corrections due to the negative effective range, in general, appear as a maximum of the gap parameter at finite momentum and a reduction of the chemical potential close to the resonance and in the BCS region. In view of the possibility of performing experiments on systems with narrow resonances, we have discussed consequences of the nonzero effective range on various measurable quantities [39]. The results presented in this work will be helpful when one explores the BCS-BEC crossover for narrow resonances.

Acknowledgments

It is a pleasure to acknowledge C. J. Pethick for stimulating discussion and his support in completing this work. We gratefully acknowledge C. E. Campbell for kindly sending us a copy of Ref. [34]. We are also grateful to G. Baym for helpful discussion in the initial stage of this work. One of the authors G. W. was partially supported by the Nishina Memorial Foundation and by the JSPS Postdoctoral Program for Research Abroad.

[1] C. A. Regal, M. Greiner, and D. S. Jin, Phys. Rev. Lett. **92**, 040403 (2004).
[2] M. W. Zwierlein, C. A. Stan, C. H. Schunck, S. M. F. Raupach, A. J. Kerman, and W. Ketterle, Phys. Rev. Lett. **92**, 120403 (2004).
[3] J. Kinast, S. L. Hemmer, M. E. Gehm, A. Turlapov, and J. E. Thomas, Phys. Rev. Lett. **92**, 150402 (2004).
[4] M. Bartenstein, A. Altmeyer, S. Riedl, S. Jochim, C. Chin, J. H. Denschlag, and R. Grimm, Phys. Rev. Lett. **92**, 203201 (2004).
[5] C. Chin, M. Bartenstein, A. Altmeyer, S. Riedl, S. Jochim, J. H. Denschlag, and R. Grimm, Science **305**, 1128 (2004).
[6] M. W. Zwierlein, J. R. Abo-Shaeer, A. Schirotzek, C. H. Schunck, and W. Ketterle, Nature **435**, 1047 (2005).
[7] D. M. Eagles, Phys. Rev. **186**, 456 (1969).
[8] A. J. Leggett, in *Modern Trends in the Theory of Condensed Matter* (Springer Verlag, 1980), p. 13.
[9] A. J. Leggett, J. de Phys., Coll. **7**, C7 (1980).
[10] G. M. Bruun and C. J. Pethick, Phys. Rev. Lett. **92**, 140404 (2004).
[11] D. S. Petrov, C. Salomon, and G. V. Shlyapnikov, Phys. Rev. A **71**, 012708 (2005).
[12] M. Bartenstein, A. Altmeyer, S. Riedl, S. Jochim, C. Chin, J. H. Denschlag, and R. Grimm, Phys. Rev. Lett. **92**, 120401 (2004).
[13] A. Perali, P. Pieri, L. Pisani, and G. C. Strinati, Phys. Rev. Lett **92**, 220404 (2004).
[14] S. Simonucci, P. Pieri, and G. C. Strinati, Europhys. Lett. **69**, 713 (2005).
[15] H. Heiselberg, Phys. Rev. Lett. **93**, 040402 (2004).
[16] H. Hu, A. Minguzzi, X.-J. Liu, and M. P. Tosi, Phys. Rev. Lett. **93**, 190403 (2004).
[17] N. Andrenacci, A. Perali, P. Pieri, and G. C. Strinati, Phys. Rev. B **60**, 12410 (1999).
[18] S. J. J. M. F. Kokkelmans, J. N. Milstein, M. L. Chiofalo,

R. Walser, and M. J. Holland, Phys. Rev. A **65**, 053617 (2002).

[19] J. Carlson, S. Y. Chang, V. R. Pandharipande, and K. E. Schmidt, Phys. Rev. Lett. **91**, 050401 (2003).

[20] M. M. Parish, B. Mihaila, E. M. Timmermans, K. B. Blagoev, and P. B. Littlewood, Phys. Rev. B **71**, 064513 (2005).

[21] S. De Palo, M. L. Chiofalo, M. J. Holland, and S. J. J. M. F. Kokkelmans, Phys. Lett. A **327**, 490 (2004).

[22] R. Diener and T.-L. Ho, cond-mat/0405174 (2004).

[23] M. Holland, S. J. J. M. F. Kokkelmans, M. L. Chiofalo, and R., Phys. Rev. Lett. **87**, 120406 (2001).

[24] J. M. Blatt and J. D. Jackson, Phys. Rev. **76**, 18 (1949).

[25] H. A. Bethe, Phys. Rev. **76**, 38 (1949).

[26] S. Flügge, *Practical Quantum Mechanics* (Springer, 1999).

[27] R. B. Diener and T.-L. Ho, cond-mat/0404517 (2004).

[28] R. Haussmann, Z. Phys. B **91**, 291 (1993).

[29] M. Marini, F. Pistolesi, and G. C. Strinati, Eur. Phys. J. B **1**, 151 (1998).

[30] T. Papenbrock and G. F. Bertsch, Phys. Rev. C **59**, 2052 (1999).

[31] Under the assumption of isotropic gap, $\Delta_{\mathbf{k}} = \Delta(k)$, we can show from the gap equation that the minimum of E_k shifts from $k = 0$ when the chemical potential equals to $(m\Delta(0)/\hbar^2)\partial_k^2\Delta(0)$ and the maximum of $\psi(k)$ shifts from $k = 0$ when $\mu = 0$.

[32] In the BCS limit, the pair wave function $\psi(k) = \Delta_{\mathbf{k}}/(2E_{\mathbf{k}})$ is very narrow around $k = k_{\mathrm{F}}$ and the gap equation is hard to solve accurately by our code. This is why we do not show the result for $r_{e0}/r_0 = -1.20$ at $(k_{\mathrm{F}}a)^{-1} \lesssim -1.1$ in this figure and Fig. 11.

[33] G. M. Bruun, Phys. Rev. A **70**, 053602 (2004).

[34] C. E. Campbell, in *Condensed Matter Theories* (Nova Science, 1997), vol. 12, p. 131.

[35] G. Ortiz and J. Dukelsky, Phys. Rev. A **72**, 043611 (2005).

[36] L. Salasnich, N. Manini, and A. Parola, Phys. Rev. A **72**, 023621 (2005).

[37] Comparing the real part of the T-matrix on resonance in their two-channel model, and to the present single-channel model with the effective range expansion, we observe that r^* in [22] corresponds to $|r_e|/4$.

[38] Also for the momentum distribution and the condensate fraction discussed later, the effective range corrections in the region of $-1 \lesssim (k_{\mathrm{F}}a)^{-1} \lesssim 1$ at $n = 0.0001 r_0^{-3}$ ($k_{\mathrm{F}}r_0 \simeq 0.14$) are about a factor of two smaller than those are at $n = 0.001 r_0^{-3}$ ($k_{\mathrm{F}}r_0 \simeq 0.31$). This fact suggests that the effective range correction scales roughly as $\sim k_{\mathrm{F}}|r_{e0}|$ under density variations.

[39] The effective range corrections also affect, e.g., the equation of state (EOS). The enhancement of the attractive interaction in the BCS side due to the negative effective range, which has been discussed in Section IV E 1, would soften the EOS. We have observed this softening within the numerical accuracy. In this calculation, we assume a polytropic EOS, $P \propto n^{\gamma+1}$, where P is the pressure and γ is the polytropic index, which is given by $\gamma = 1 + n(\partial^2\mu/\partial n^2)/(\partial\mu/\partial n)$. However, the second derivative $(\partial^2\mu/\partial n^2)$ is hard to calculate accurately and our results of γ are not accurate enough to discuss quantitatively.